Jiao, Hairui; Xu, Guifeng; Sang, Yushuai; Chen, Hong; Li, Yongdan

Direct conversion of enzymatic hydrolysis lignin to cycloalkane fuel with hydrotalcite-derived Ni catalyst

Published in:
Catalysis Today

DOI:
10.1016/j.cattod.2024.114542

Published: 15/03/2024

Document Version
Publisher's PDF, also known as Version of record

Catalysis Today 430 (2024) 114542

Contents lists available at ScienceDirect

Catalysis Today

journal homepage: www.elsevier.com/locate/cattod

Direct conversion of enzymatic hydrolysis lignin to cycloalkane fuel with hydrotalcite-derived Ni catalyst

Hairui Jiao [a], Guifeng Xu [b], Yushuai Sang [c,*], Hong Chen [b,*], Yongdan Li [c]

[a] Collaborative Innovation Center of Chemical Science and Engineering, Tianjin Key Laboratory of Applied Catalysis Science and Technology, State Key Laboratory of Chemical Engineering, School of Chemical Engineering, Tianjin University, Tianjin 300072, China
[b] School of Environmental Science and Engineering, Tianjin University, Tianjin 300072, China
[c] Department of Chemical and Metallurgical Engineering, School of Chemical Engineering, Aalto University, Kemistintie 1, Espoo FI-00076, Finland

ARTICLE INFO

Keywords:
Biofuel
Nickel catalyst
Enzymatic hydrolysis lignin
Hydrodeoxygenation
Hydrotalcite precursor

ABSTRACT

Herein, we reported a one-pot method that directly converting enzymatic hydrolysis lignin (EHL) into cycloalkane fuels using a Ni catalyst derived from Ni-Al hydrotalcite (NiAl-LDH). The effects of Ni/Al ratio and reduction condition on the catalytic activity have been examined. The catalyst obtained from the reduction of NiAl-LDH at 460 °C (Ni_2Al_1-re460) shows the highest activity among the catalyst samples examined, attributed to its abundant Lewis acidic sites, small-sized Ni metal particles, and large specific surface area. At optimized reaction conditions (320 °C, 3 MPa H_2, 6 h), this catalyst achieves 100% EHL conversion and complete oxygen removal and improves the calorific value of the products from 25.0 MJ kg^{-1} to 42.5 MJ kg^{-1}. The detected products are cycloalkane dimers and monomers with their carbon numbers within the range suitable for gasoline and diesel, and other large molecules with uncertain structures also predominantly consist of cycloalkane rings.

1. Introduction

Due to the concerns about the reserves and environmental pollution from fossil fuel combustions, it is crucial to find sustainable energy sources and chemical production processes based on renewable resources. Lignin is a key component of biomass, which is composed of three benzene propane units, including p-hydroxyphenyl (H), guaiacyl (G), and syringyl (S), randomly linked with C-O-C and C-C bonds [1,2]. Enzymatic hydrolysis lignin (EHL) emerges as a by-product in the 2nd generation bioethanol production industry [3,4]. Due to its aromatic nature, EHL holds promise as a viable alternative to petroleum for the production of chemicals and fuels. Nevertheless, the depolymerization of EHL into small molecules remains a challenge because of its complex structure and chemical inertness [5].

Catalytic lignin alcoholysis presents a promising approach for depolymerizing lignin into valuable small molecules. In our previous works, Kraft lignin has been completely depolymerized into small molecules via catalytic alcoholysis using Mo-based catalysts [6–11]. Recently, we examined catalytic EHL alcoholysis with different catalysts. Mai et al. [12] employed WO_3/Al_2O_3 as a catalyst for EHL ethanolysis under N_2 atmosphere at 320 °C and obtained 32 wt% yields of phenolic monomers, primarily complex alkylphenols. Sang et al. [13,14] developed unsupported Ni catalysts for EHL ethanolysis and obtained 28 wt% yields of aromatic esters and alkylphenols at 280 °C under 2 MPa H_2. Ma et al. [15] investigated the activity of MoS_2 in EHL ethanolysis at 320 °C under N_2 atmosphere and obtained a high yield of 2-(tert-butyl)−3-methylphenol. Although these studies achieved complete EHL conversion and high monomer yields, a notable drawback was the high oxygen content in the obtained products. Therefore, additional upgrading, particularly hydrodeoxygenation (HDO), is necessary to remove methoxyls, hydroxyls, and other oxygenated side chains in the products [16,17].

HDO of lignin-derived phenolics, such as phenol and guaiacol, has been intensively investigated for nearly two decades, and different catalysts have been developed, including Ni and noble metal catalysts, Ni and Co-based phosphides, and Mo and W-based sulfides, carbides, nitrides and oxides [18–20]. Among these catalysts, Ni and noble metal catalysts exhibit higher hydrogenation activity and typically produce cycloalkanes as the main products [18–20]. Recently, a one-pot method combining lignin depolymerization and simultaneous HDO of the products has been developed [21–29]. Noble metal catalysts, such as Ru/Al_2O_3, $Pd/NbOPO_4$, $Ru/NbOPO_4$ and Pt/HAP, show high activities for lignin HDO reactions, due to their superior hydrogenation activities [26–30]. However, these noble metal catalysts require a high loading of

* Corresponding authors.
E-mail addresses: yushuai.sang@aalto.fi (Y. Sang), chenhong_0405@tju.edu.cn (H. Chen).

https://doi.org/10.1016/j.cattod.2024.114542
Received 28 November 2023; Received in revised form 21 December 2023; Accepted 19 January 2024
Available online 23 January 2024

up to 5 wt% to achieve complete lignin conversion and maximize hydrocarbon yields. Despite their excellent performance, the high cost of noble metal catalysts limits their practical application [19]. In our recent work, we employed $NiMo/Al_2O_3$ for the direct HDO of EHL, achieving complete EHL conversion and a yield of 104.4 mg g^{-1} of cycloalkanes at 320 °C under 3 MPa H_2 [31]. Although this result presents a promising alternative for lignin HDO reaction with a cost-effective Ni-based catalyst, a novel catalyst with higher activity needs to be further developed.

Hydrotalcite-derived catalysts have been widely employed in many industrial chemical reactions. For lignin depolymerization reaction, significant advancements have been made using hydrotalcite-derived catalysts, achieving complete lignin liquefaction and high yields of monomers [11,32,33]. In this work, Ni catalysts derived from Ni-Al hydrotalcite were employed for the HDO reaction of EHL in cyclohexane solvent. The effects of Ni/Al ratio and the reduction temperature of the catalyst on the activity have been investigated. The reaction parameters are also optimized to obtain a high yield of cycloalkanes. At optimized reaction conditions, 100% EHL conversion and complete oxygen removal were achieved, direct conversing EHL to cycloalkane fuels. This research presents a promising method for producing renewable biofuels from the solid waste generated in the biomass refining process.

2. Experimental

2.1. Materials

The EHL was purchased from Shandong Longlive Biotechnology Co. Ltd, and has been characterized in our previous work [13,14,34]. The content of lignin in EHL is 91.2 wt% and the carbon content of EHL is 61.3 wt%, respectively. Analytical reagents (AR), including cyclohexane (CYH), veratrole, $Ni(NO_3)_2{\cdot}6\ H_2O$, $Al(NO_3)_3{\cdot}9\ H_2O$, and urea were purchased from Aladdin Co. Ltd. and used as received. The water was provided by an ultrapure water purification system (UPH-1–10). The gases used in this work include H_2 (99.999 vol%), Ar (99.9 vol%), He (99.5 vol%), and N_2 (99.999 vol%). Moreover, the air was supplied with an air pump.

2.2. Catalyst preparation and characterization

The synthetic route of the catalyst precursor is as follows. $Ni(NO_3)_2{\cdot}6\ H_2O$ (21.2 g), $Al(NO_3)_3{\cdot}9\ H_2O$ (13.6 g) and urea (47.1 g) are completely dissolved in de-ionized water (120 mL), and the solution is heated at 105 °C for 12 h with vigorous stirring in a three-necked bottle, and aged at 60 °C for 24 h. After that, the precipitate is separated through filtration and washed with de-ionized water and then dried at 110 °C. To investigate the role of Al species on the catalyst structure, catalysts with different molar ratios of Ni/Al were prepared following the above procedure, and the samples were denoted as Ni_xAl_y. The Ni_xAl_y was reduced at different temperatures (460, 520, and 580 °C) for 4 h to obtain the catalyst and named as Ni_xAl_y-reT (T = 460, 520, 580 °C). To prevent oxidation before characterization, the catalyst underwent passivation at room temperature in 5% O_2/95%Ar and was subsequently stored in sealed containers purged with pure N_2.

The X-ray powder diffraction (XRD) patterns are collected with the Bruker D8-Focus diffractometer (Cu Kα, λ = 1.5406 Å) at 40 kV and 40 mA from 20° to 80° at a speed of 8° min^{-1}. The morphology and structure of samples are observed with a scanning electron microscope (SEM, S-4800, JEOL) and a transmission electron microscope (TEM, JEM-2100 F, Hitachi). The specific surface area of a sample is measured with the nitrogen adsorption-desorption at − 196 °C and analyzed with the multipoint BET method (Quantachrome Auntosorb^{-1}). Before the nitrogen adsorption-desorption test, the samples are pre-treated at 300 °C for 3 h under a vacuum. The X-ray photoelectron spectroscopy (XPS) was performed with a PHI-1600 ESCA system spectrometer using Mg Kα as the X-ray source (1253.6 eV) under a residual pressure of 5×10^{-6} Pa, with the binding energy calibrated using C1s at 284.8 eV as the internal standard. The Fourier transform infrared spectra of pyridine adsorption (Py-IR) were recorded on a Tensor 27 infrared spectrometer. The catalyst was first heated in a vacuum at 350 °C for 1 h and then cooled to 50 °C for the record of background spectra. After that, the sample was exposed to the pyridine vapor at 50 °C for 1 h and then treated in a vacuum at 150 °C for 1 h to remove the physically adsorbed pyridine. The Py-IR spectrum was recorded in the 1400–1700 cm^{-1} range after the sample was cooled down to room temperature. A thermogravimetric analyzer (TG, PE TGA) was used to determine the weight of adsorbed species on the catalyst after the reaction. The sample was heated from 50 °C to 650 °C at a rate of 5 °C min^{-1} in N_2 (80 mL min^{-1}). The Raman spectra of samples were obtained on Raman spectrometer (Raman, HORIBA LabRAM HR Evolution, France) using excitation light at 532 nm as the light source and a scan range of 1400–1700 cm^{-1}.

2.3. Reaction condition

The reaction is carried out in a 300 mL batch reactor (Parr 4566, made of Hastelloy) equipped with a temperature controller (Parr 4848) and a pressure sensor. In a typical run, EHL (1.0 g), catalyst (0.5 g), and solvent (100 mL) were loaded into the reactor. After six purges with nitrogen and three purges with hydrogen, the reactor was filled with a prescribed hydrogen pressure. The sealed reactor was then heated to the prescribed temperature with the stirring fixed at 600 rpm for a prescribed time. After the reaction, the reaction mixture is filtrated to separate the liquid product and solid residue.

2.4. Product analysis

The liquid product was quickly injected into an Agilent 6890–5973 GC-MS system and an Agilent 6890 GC equipped with FID for qualitative and quantitative analysis, respectively. Both GC and GC-MS were operated under the same conditions. The columns used in both GCs were HP-5 MS capillary columns. The ramp-up procedure was set to increase from an initial temperature of 45 °C at a rate of 10 °C min^{-1} to a final temperature of 250 °C. The column was held at 250 °C for 7 mins. The split ratio was set to 50. The mass detector was set to scan from 10 to 500 *m/z*. The identification of the compounds was achieved with GC-MS by comparing the obtained mass spectra with those in the database (NIST02). Veratrole is used as the internal standard for the quantitative analysis of products. The total product yield is expressed as mg/g EHL and is calculated with Eq. (1).

$$\text{Total product yield of EHL reaction (mg g}^{-1}\text{EHL)} = \frac{\text{The mass weight of total products}}{\text{The mass weight of the initial EHL}} \quad (1)$$

The solid residue was washed with ethanol and then dried in vacuum oven at 60 °C. EHL conversion is calculated with Eq. (2), in which "the mass weight of recovered catalyst" is obtained from the blank reaction without EHL.

$$\text{EHL conversion (wt\%)} = \left(1 - \frac{\text{The mass weight of solid residue} - \text{the mass weight of recovered catalyst}}{\text{The mass weight of the initial EHL}}\right) \times 100\% \quad (2)$$

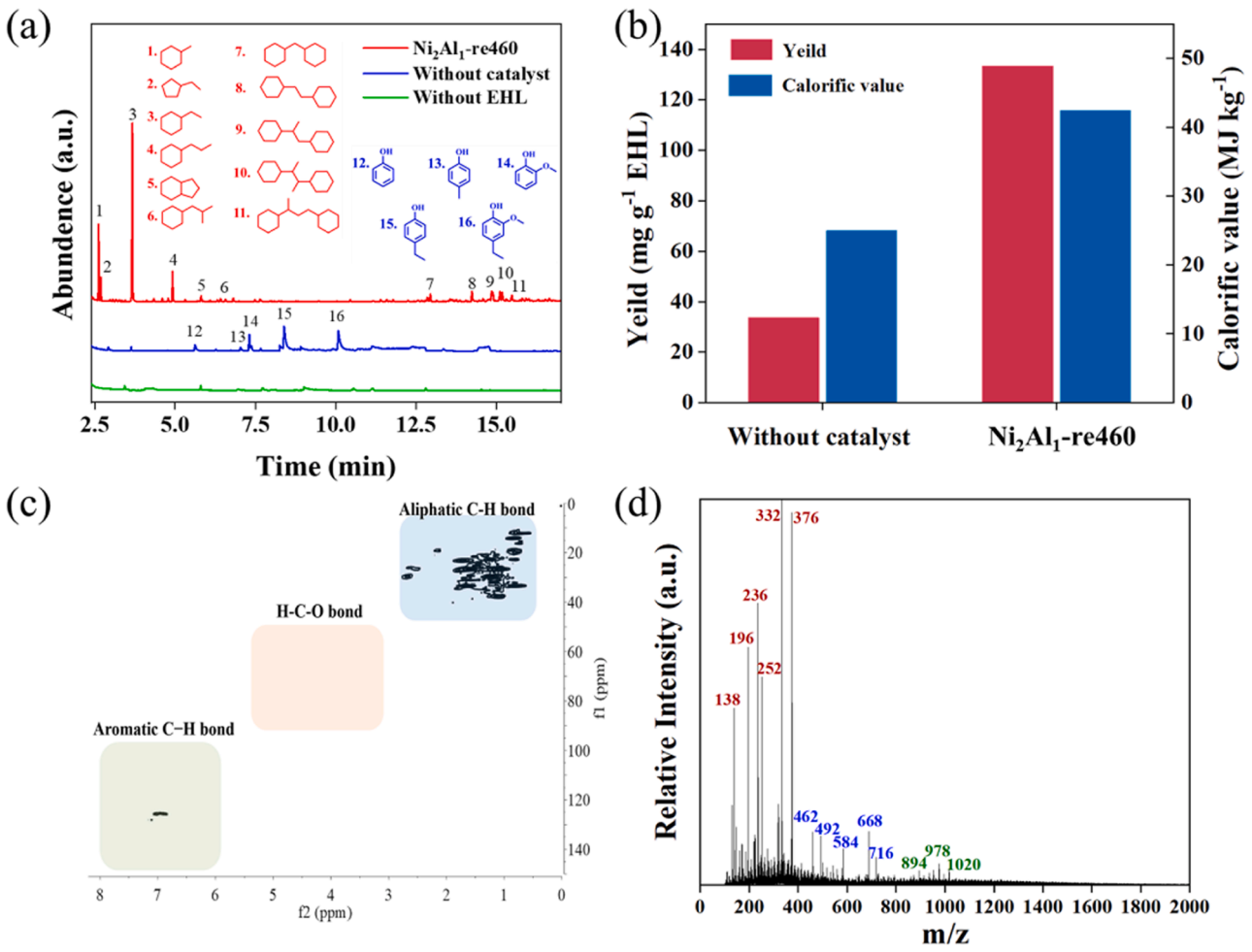

Fig. 1. (a) The structures of the detected product obtained from EHL conversion without catalyst and with Ni_2Al_1-re460 catalyst. (b) The total yield of the detected product and the calorific value of the whole product mixture with solvent obtained from EHL conversion without catalyst and with Ni_2Al_1-re460 catalyst. (c) HSQC NMR and (d) MALDI-TOF-MS spectra of the product mixture from EHL conversion with Ni_2Al_1-re460 catalyst. (Reaction condition: 1.0 g EHL, 0.5 g catalyst or without catalyst, 100 mL CYH, 320 °C, 3 MPa initial H_2 pressure, 6 h).

Heteronuclear single quantum coherence-nuclear magnetic resonance (HSQC NMR) spectra were recorded on a Bruker AVANCE III HD 400 MHz. The solvent in the product mixture was removed by evaporation, and then the liquid residue was dissolved in 0.5 mL of DMSO-d_6 as the deuteration NMR solvent. The matrix-assisted laser desorption/ionization time-of-flight mass spectrometry (MALDI-TOF-MS) analysis of liquid residue was measured with an Autoflex tof/toflll equipment made by American Bruker Dalton Corporation. A 15 g/L solution of 2, 5-dihydroxyl benzoic acid (DHB) (Sigma) in ethanol was used as a matrix.

3. Results and discussion

3.1. Catalytic activity

The performance of Ni_2Al_1-re460 catalyst in the HDO reaction of EHL was evaluated in CYH at 320 °C for 6 h under 3 MPa H_2. As shown in Fig. 1(a) and (b), this catalyst only produces cycloalkanes, including monomers and dimers, with a total yield of 133.2 mg g^{-1} EHL. As all of the oxygen has been removed in the detected products, the total yield of cycloalkanes is also calculated based on the carbon content of EHL, and this value is 21.7 wt%. The detected monomers, mainly including methyl-, ethyl-, and propyl-cycloalkanes, are well-suited as additives for gasoline, and the detected dimers with carbon numbers ranging from C13 to C16 are suitable as additives for diesel. In contrast, the reaction without a catalyst only produced phenolic compounds with a total yield of 33.6 mg g^{-1} EHL. The liquid product obtained without a catalyst exhibits a brown color, while the product obtained with the Ni_2Al_1-re460 catalyst appears as a colorless liquid, indicating the removal of oxygen-containing functional groups (Fig. S1). In addition, with the introduction of the Ni_2Al_1-re460 catalyst, the calorific value of the products increased significantly from 25.0 MJ kg^{-1} to 42.5 MJ kg^{-1}. CYH is stable during the reaction and no products were detected in the absence of EHL feedstock, indicating that the catalyst cannot open the cycloalkane ring.

CYH is also a major product derived from the HDO reaction of lignin, but it cannot be identified when it is used as the solvent in this study. We also tested other alkanes, including n-pentane and n-dodecane, as solvents. However, the reaction pressure became too high when n-pentane was used, necessitating the termination of the experiment, due to its low boiling point (36.7 °C). On the other hand, n-dodecane was unstable under our reaction conditions, and the alkanes derived from n-dodecane interfered with product analysis. Therefore, CYH was selected as the solvent for further investigation, despite the fact that it leads to an underestimation of the product yield.

GC-MS analysis is limited to detecting only the monomer and dimer products. Hence, HSQC NMR and MALDI-TOF-MS are employed to characterize the structure and molecular weight distribution of the whole product mixture, respectively. In the HSQC NMR spectrum of

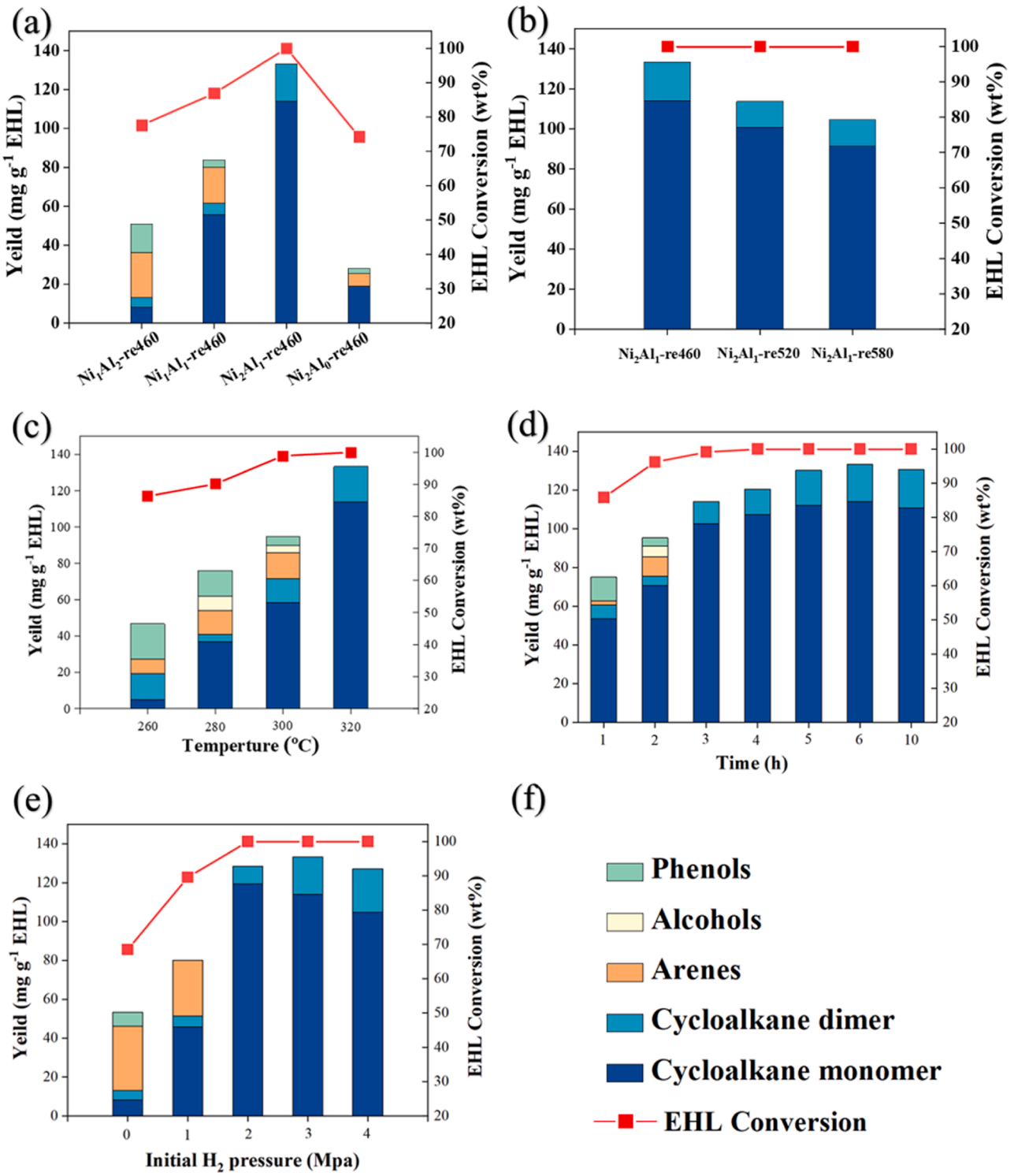

Fig. 2. The product yields obtained with catalysts at different molar Ni/Al ratios (a) and reduced under different temperatures (b). The effects of reaction temperature (c), time (d), initial H_2 pressure (e) on the product yields with Ni_2Al_1-re460 catalyst. (Reaction condition: 1.0 g EHL, 0.5 g catalyst, 100 mL CYH).

product mixture obtained with the Ni_2Al_1-re460 catalyst (Fig. 1(c)), the signals of aromatic C-H bonds are significantly attenuated, and the signals corresponding to C-O bonds disappear, while the signals of aliphatic C-H bonds are enhanced, compared to that of original EHL (Fig. S2). These results indicate that the O in the product mixture has been completely removed, and most of benzene rings are hydrogenated and the molecules primarily consist of cycloalkane rings. The MALDI-TOF-MS spectrum of the product mixture is shown in Fig. 1(d). The molecules with *m/z* in the range of 100–400 are the major products, with carbon numbers in the range suitable for gasoline and diesel. The product mixture also contains small amounts of molecules with *m/z* in the range of 450–750 and trace amounts of molecules with *m/z* in the range of 900–1050.

By comparing the direct HDO conversion of lignin or biomass to hydrocarbons (Table S1), it is found that the catalytic activity of Ni_2Al_1-re460 is comparable to that of precious metal-based catalysts in terms of

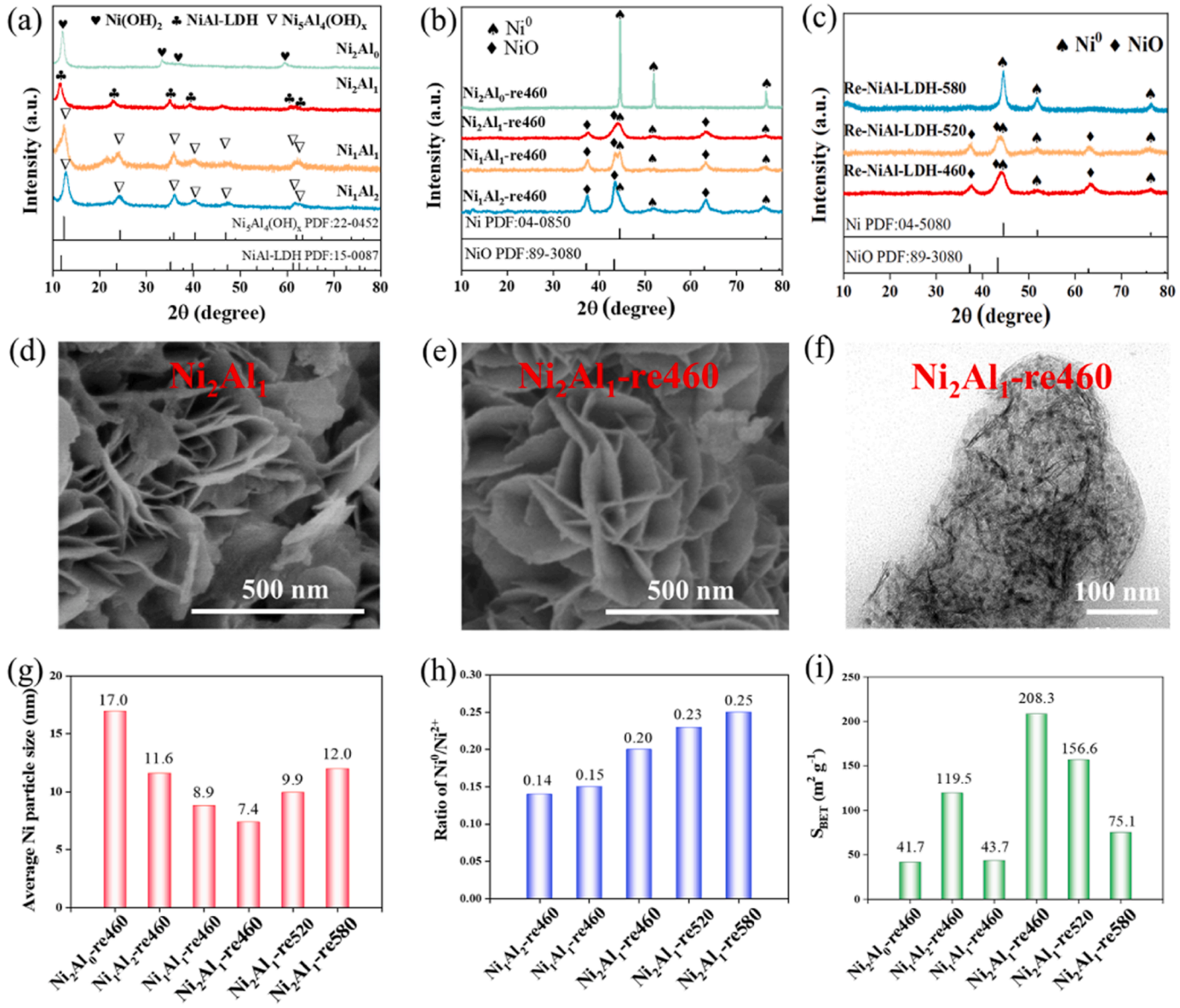

Fig. 3. XRD patterns of catalysts with different Ni/Al molar ratios before (a) and after reduction (b) and reduced Ni_2Al_1 at different reduction temperatures (c). SEM images of (d) Ni_2Al_1 and (e) Ni_2Al_1-re460. (f) TEM image of the Ni_2Al_1-re460 catalyst. (g) Average Ni particle size counted according to TEM images. (h) The ratios of surface Ni^0 to Ni^{2+} species of reduced catalysts determined with XPS analysis. (i) The specific surface area of reduced catalysts calculated with the BET method.

the yield of hydrocarbons. At the same time, a significant increase in the calorific value of EHL is realized, exclusively yielding cycloalkanes at 100% EHL conversion.

3.2. Effect of Ni/Al ratio and reduction temperature

The activities of the catalysts with different Ni/Al ratios reduced at 460 °C (Ni_1Al_2-re460, Ni_1Al_1-re460, Ni_2Al_1-re460, and Ni_2Al_0-re460) and reduced Ni_2Al_1 at different temperatures (Ni_2Al_1-re460, Ni_2Al_1-re520 and Ni_2Al_1-re580) are shown in Fig. 2(a) and (b), respectively. Among the catalysts with different Ni/Al ratios, the Ni_2Al_1-re460 catalyst achieves complete EHL conversion and the highest total product yield of 133.2 mg g^{-1} EHL, with only cycloalkane monomers and dimers as detected products. In contrast, when Ni_1Al_2-re460, Ni_1Al_1-re460 and Ni_2Al_0-re460 are used, EHL is not completely converted, and the total product yields obtained are much lower than that obtained with Ni_2Al_1-re460. In addition, these catalysts also show low activities for HDO reaction, as high amounts of phenols and arenes are detected. The increase of reduction temperature from 460 to 580 °C of Ni_2Al_1 catalyst does not affect the EHL conversion, which remained at 100.0 wt%, and product distribution, which only contains cycloalkanes, but reduces the total product yield from 133.2 to 104.6 mg g^{-1} EHL.

3.3. Effect of reaction conditions

The effects of reaction temperature, time, and initial H_2 pressure on the product yield and distribution are examined with Ni_2Al_1-re460 as the catalyst, and the results are shown in Fig. 2(c-e).

The effect of reaction temperature was examined with the reaction time and initial H_2 pressure fixed at 6 h and 3 MPa, respectively. At 260 °C, the EHL conversion and total product yield are only 86.3 wt% and 46.8 mg g^{-1} EHL, respectively, and high contents of unsaturated products (phenols and arenes) are produced. With the increase of the reaction temperature from 260 to 320 °C, both the EHL conversion and total product yield increase , indicating the enhancement of EHL depolymerization. Moreover, the increase in reaction temperature also

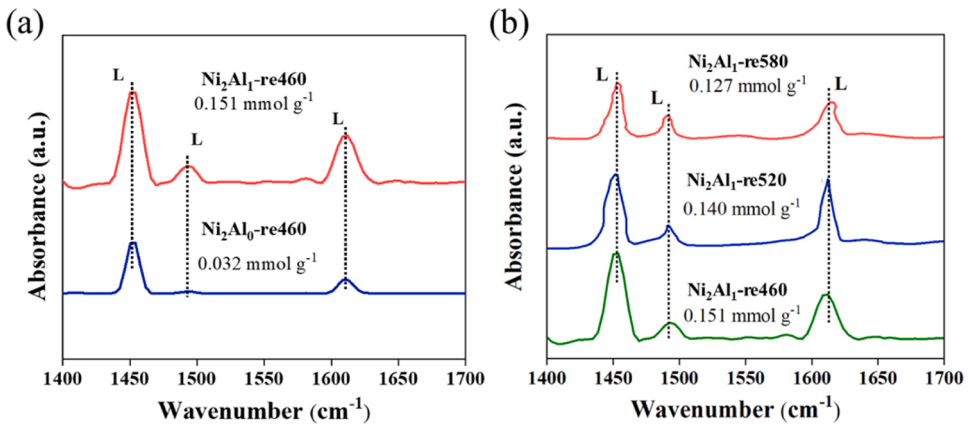

Fig. 4. Py-IR spectra of (a) Ni_2Al_1-re460 and Ni_2Al_0-re460, and (b) reduced Ni_2Al_1 at different reduction temperatures.

promotes HDO reaction, which leads to the transformation of unsaturated products into cycloalkanes. At 320 °C, the EHL conversion and total product yield reach the maximum values, and only cycloalkane monomers and dimers are detected.

The effect of reaction time was examined with the reaction temperature and initial H_2 pressure fixed at 320 °C and 3 MPa, respectively (Fig. 2(d)). When the reaction time is 1 h, cycloalkanes have been the main products (56.2 mg g^{-1} EHL) and the EHL conversion has been up to 85.8 wt%. With the reaction time extending to 2 h, alcohols are detected, and the yields of arenes and cycloalkanes increase, but the yield of phenols decreases. Further increasing the reaction time to 3 h, only cycloalkanes and cycloalkane dimer are detected and the EHL conversion is up to 100 wt%. Hence, phenols are the primary products that are converted into alcohols and arenes and further converted into cycloalkanes during a 3 h reaction. From 3 to 6 h, the yield of cycloalkane dimer increases from 11.5 to 19.3 mg g^{-1} EHL, more obvious than the yield of cycloalkane monomer. This indicates that the HDO reaction rates of lignin dimers are slower than that of lignin monomers. The HDO of lignin monomers is nearly completed in 3 h, but the HDO of lignin dimers is gradually completed over 6 h.

The effect of initial H_2 pressure was examined with the reaction temperature and time fixed at 320 °C and 6 h, respectively (Fig. 2(e)). When the initial H_2 pressure is 0 MPa, the EHL conversion is only 68.5 wt% and high yield of arenes and small amounts of phenols and cycloalkanes are produced with a total yield of 53.4 mg g^{-1} EHL. The increase of the initial H_2 pressure facilitates both EHL depolymerization and product HDO reaction. At 2 MPa H_2, a total product yield of 128.5 mg g^{-1} was obtained at 100 wt% EHL conversion, and only cycloalkane monomers and dimers are produced. Interestingly, a further increase of the initial hydrogen pressure from 2 MPa to 4 MPa leads to a decrease in the cycloalkane monomer yield, but an increase in the cycloalkane dimer yield. The reason may be that the hydrogenolysis of lignin dimers to monomers over the catalyst is hindered by the adsorption of H_2 at high hydrogen pressure [35].

3.4. Catalyst characterization

Fig. 3(a) shows the XRD patterns of catalyst precursors with different ratios of Ni and Al (Ni_1Al_2, Ni_1Al_1, Ni_2Al_1, and Ni_2Al_0) before reduction. Ni_2Al_1 exhibits diffraction peaks corresponding to NiAl-LDH (PDF #15–0087). However, in the patterns of Ni_1Al_2 and Ni_1Al_1, no diffraction peaks of NiAl-LDH were found but peaks of $NiAl(OH)_x$ (PDF #22–0452) were observed. In the XRD pattern of Ni_2Al_0, only the peaks related to α-$Ni(OH)_2$ appear. Therefore, NiAl-LDH can only be synthesized at Ni/Al= 2 under this condition. The XRD patterns of the reduced catalysts at 460 °C (Ni_1Al_2-re460, Ni_1Al_1-re460, Ni_2Al_1-re460 and Ni_2Al_0-re460) are shown in Fig. 3(b). Both the peaks of NiO and Ni are observed in the XRD patterns of Ni_1Al_2-re460, Ni_1Al_1-re460, and Ni_2Al_1-re460, but only the peaks attributed to Ni appear in the XRD patterns of Ni_2Al_0-re460. In addition, the diffraction peaks of Ni in Ni_2Al_0-re460 are more intense compared to those in Ni_1Al_2-re460, Ni_1Al_1-re460, and Ni_2Al_1-re460, indicating that larger Ni particles form in Ni_2Al_0-re460. Fig. 3(c) shows the XRD patterns of Ni_2Al_1 reduced at different temperatures (460, 520, and 580 °C). The XRD patterns of Ni_2Al_1-re460 and Ni_2Al_1-re520 are similar, in which both the peaks of NiO and Ni are observed. The coexistence of Ni and NiO on Ni_2Al_1-re460 is also confirmed by its SAED pattern (Fig. S3). Nevertheless, in the XRD pattern of Ni_2Al_1-re580, the peaks of NiO are nearly invisible and the peaks of Ni are more intense compared to those in Ni_2Al_1-re460 and Ni_2Al_1-re520.

Fig. 3(d) and (e) display the SEM images of Ni_2Al_1 before and after reduction at 460 °C. Ni_2Al_1 has distinct lamellar structures, and these lamellar structures are maintained after reduction at 460 °C. The stacked layered structures in Ni_2Al_1-re460 result in the formation of large pores, which are favorable for the adsorption of lignin macromolecules. Nevertheless, Ni_1Al_2, Ni_1Al_1, and Ni_2Al_0 samples do not show a lamellar structure before and after reduction (Figs. S5 (a) and (b)). The high reduction temperature (520 and 580 °C) of Ni_2Al_1 results in the collapse of the lamellar structures (Fig. S6 (a)). Fig. 3(f) displays the TEM image of Ni_2Al_1-re460. Black particles on the catalyst surface are identified as Ni particles according to their lattice fringes (Fig. S4). The average Ni particle sizes of different reduced catalysts are counted according to their TEM images (Fig. 3(f), Fig. S5 (c) and Fig. S6 (b)), and the results are shown in Fig. 3(g). Among the Ni_1Al_2-re460, Ni_1Al_1-re460, and Ni_2Al_0-re460 samples, Ni_2Al_1-re460 has the smallest Ni particle size (7.4 nm), indicating that the employment of NiAl-LDH precursor efficiently restrains the growth of Ni particle size during the reduction process. The increase of the reduction temperature from 460 to 580 °C results in the increase of average Ni particle size from 7.4 to 12.0 nm.

The ratios of Ni^0 to Ni^{2+} species on the surface of reduced catalysts are determined with XPS analysis (Fig. S7), and the results are shown in Fig. 3(i). The ratio of surface Ni^0/Ni^{2+} species gradually decreased from 0.20 to 0.14 with the decrease of Ni/Al ratio from 2/1 to 1/2, indicating that the reduction degree of Ni decreases with the increase of Al content. The Ni_2Al_1-re460 with a higher Ni reduction degree shows a higher hydrogenation activity. With the increase of the reaction temperature, the Ni^0/Ni^{2+} ratio increases, and Ni_2Al_1-re580 has more surface Ni^0 species than Ni_2Al_1-re480 and Ni_2Al_1-re520. However, the large Ni particles due to the sintering of Ni at 580 °C result in the low hydrogenation activity of Ni_2Al_1-re580.

The specific surface areas of reduced catalysts are shown in Fig. 3(i). Owing to its LDH structure, Ni_2Al_1-re460 has a high specific surface area (208.3 m^2 g^{-1}), much higher than that of Ni_2Al_0-re460, Ni_1Al_2-re460 and Ni_1Al_1-re460 samples. With the increase of the reduction

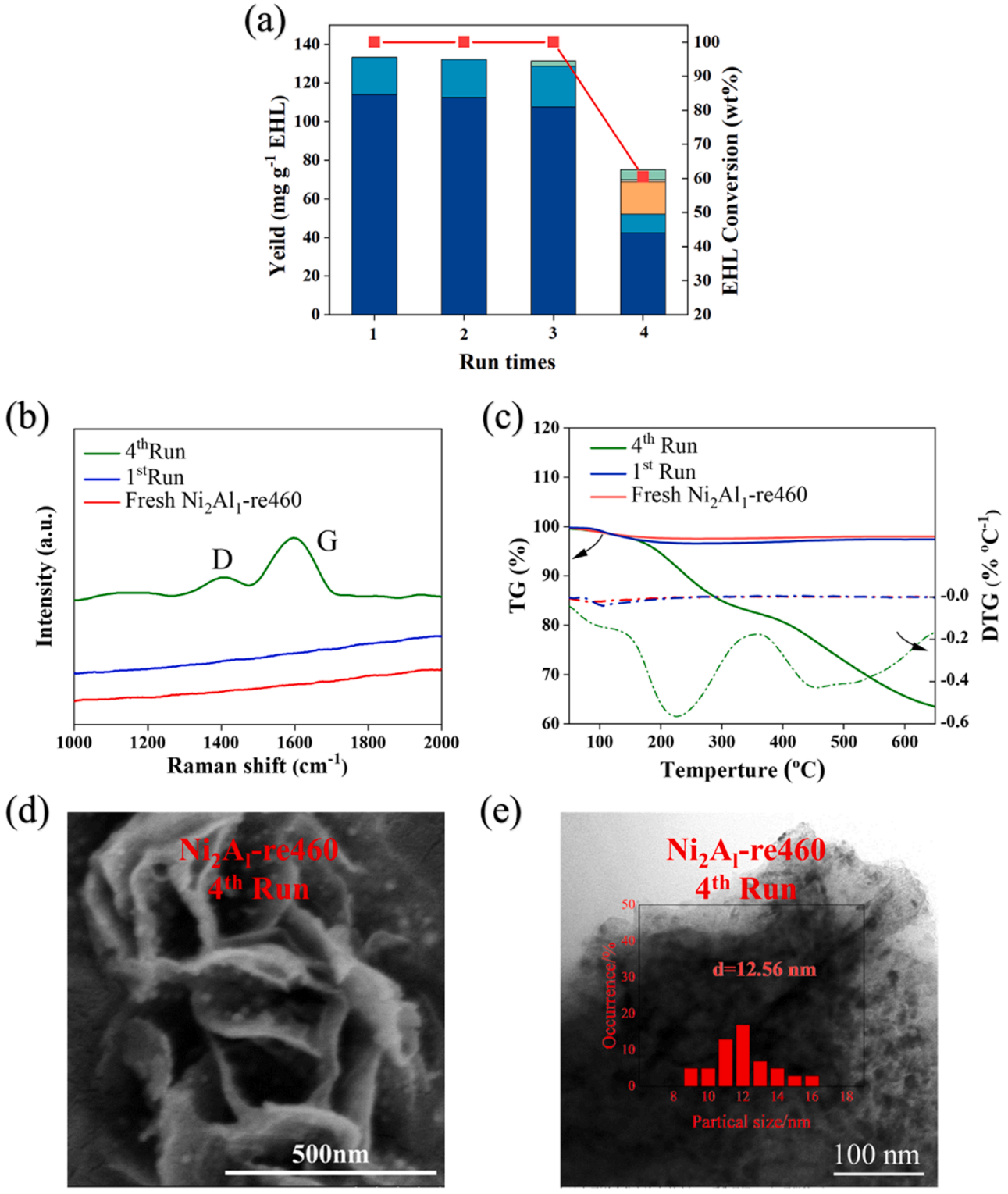

Fig. 5. Recycle of the Ni_2Al_1-re460 catalyst (a). Raman spectra (b) and TG curves (c) of fresh, first and fourth used Ni_2Al_1-re460 catalyst in N_2. SEM (d) and TEM (e) images of fourth used Ni_2Al_1-re460 catalyst.

temperature from 460 to 580 °C, the specific surface area of catalysts is significantly reduced from 208.3 to 75.1 $m^2\ g^{-1}$ due to the collapse of the lamellar structures (Fig. S6 (a)).

The acidity of catalysts also plays an important role in HDO reactions. Py-IR was used to analyze the surface acidic sites of reduced catalysts, and the results are shown in Fig. 4. In all of these spectra, only the peaks ascribed to the vibration absorption of pyridine adsorbed on Lewis acid sites (1450, 1490 and 1610 cm^{-1}) are observed, while the peak related to the Brønsted acid sites does not appear at 1535 cm^{-1} [36–39]. Therefore, the reduced catalysts only have Lewis acid sites. The amount of Lewis acid sites on Ni_2Al_1-re460 is 0.151 mmol g^{-1}, much higher than that on Ni_2Al_0-460, which is only 0.032 mmol g^{-1}. Hence, the addition of Al significantly improves the amount of Lewis acid sites on the catalyst. In Ni_2Al_1-re460, Al and Ni species cannot be completely

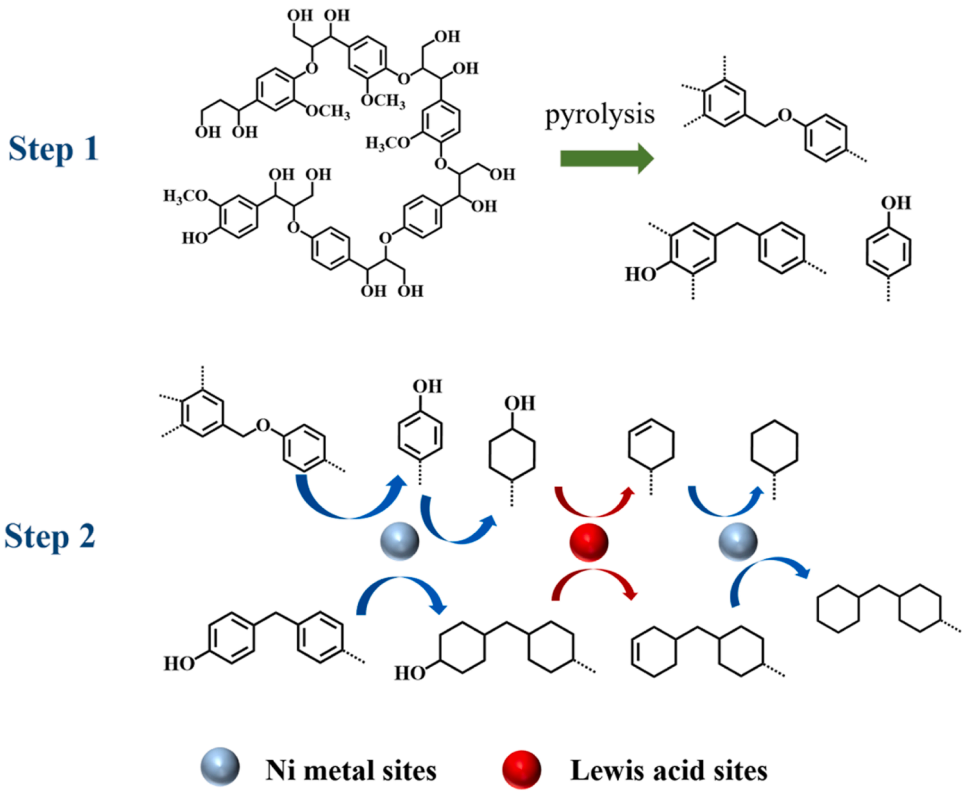

Scheme 1. Reaction pathways of the direct HDO of EHL.

reduced at our reduction condition, and oxygen vacancies formed after reduction serves as Lewis acid sites. With the increase of reduction temperature from 460 to 580 °C, the amount of Lewis acid sites gradually decreases from 0.151 to 0.127 mmol g^{-1} due to the reduction of more Ni species to metal Ni.

3.5. Catalyst stability

The stability of Ni_2Al_1-re460 was examined and the results are shown in Fig. 5(a). The EHL conversion, total product yield, and product distributions are not obviously changed in two times run. In the 3th run, the catalyst slightly loses its activity, yielding 8.7 mg g^{-1} EHL of phenols at 100 wt% EHL conversion. Nevertheless, in the 4th run, the EHL conversion and total product yield significantly decrease to 60.0 wt% and 75.2 mg g^{-1} EHL, respectively, and 21.8 mg g^{-1} EHL yield of phenols is detected, indicating the deactivation of the catalyst.

The Ni/Al ratio showed no significant difference between the fresh and 4th used catalysts (Fig. S8), indicating negligible Ni species leaching during reusability tests. The Raman spectra of used catalysts (Fig. 5(b)) indicate that carbon deposition has occurred on the 4th used catalyst but not on the 1st used catalyst. The TG and DTG curves of the fresh catalyst as well as the 1st and 4th used catalysts in N_2 are shown in Fig. 5(c). From 50 to 650 °C, there is no weight loss for the fresh and the first used catalyst, but the weight loss of 4th used catalyst is up to 35%. The DTG curve of the 4th used catalyst has two peaks at 220 °C and 450 °C, which may be attributed to the desorption of lignin fragments and large condensed structures from the catalyst, respectively [40,41]. Fig. 5(d) and (e) show the SEM and TEM images of the 4th used catalyst. After 4 runs, the catalyst keeps its lamellar structure, but carbon particles are observed on the catalyst, and the average Ni particle size increases to 12.56 nm.

4. Discussion

4.1. Reaction pathways

In the previous works about lignin depolymerization in alcohol, lignin alcoholysis was considered to be the first step, in which alcohol was decomposed into active H and ethoxy, which depolymerized lignin to fragments and monomers [8,42,43]. For EHL depolymerization in CYH, the non-catalytic reaction that depolymerizes EHL to lignin fragments and monomers should be also the first step, because large lignin molecules cannot directly contact the solid catalyst. However, our results indicate that CYH remains stable under our reaction conditions and does not generate active groups that facilitate lignin solvolysis. This suggests that the non-catalytic reaction of EHL may be a thermal decomposition process (Scheme 1, step 1) [25]. The role of CYH is to dissolve lignin fragments and monomers produced through the pyrolysis process, suppressing their condensation reactions.

The second step is further depolymerization of lignin fragments and HDO of dimers and monomers over a catalyst (Scheme 1, step 2). Lignin fragments containing C-O-C linkages undergo hydrogenolysis, producing phenolics that are subsequently hydrogenated into cycloalkanols over the Ni metal sites. The cycloalkanols are then dehydroxylated over Lewis acid sites and finally hydrogenated into cycloalkanes over the Ni metal sites. The catalyst may not be able to depolymerize fragments with C-C linkages but converts them into cycloalkane dimer. Consequently, cycloalkane dimers with C-C linkages are identified in the products of EHL conversion. The HDO of lignin fragments to cycloalkanes shifts the solubility equilibrium of lignin fragments in CYH and hence hinders their condensation to char [23].

4.2. The activity of catalyst

The catalysts derived from NiAl-LDH (Ni_2Al_1-re460) show higher activities than catalysts without LDH structures (Ni_1Al_2-re460, Ni_1Al_1-

re460, and Ni_2Al_0-re460). The presence of the NiAl-LDH phase leads to maximum specific surface area and the formation of large pores, which facilitates reactant adsorption [44]. The interaction between Ni and Al facilitates the formation of small metal Ni particles, resulting in the high hydrogenation activity of the catalyst. Moreover, due to the Ni-Al interaction, only a portion of Ni in NiAl-LDH is reduced to metal Ni nanoparticles, while the partially reduced Al and Ni act as Lewis acid sites, which absorb oxygen-containing functional groups in the reactants and promote the deoxygenation reaction [45–47]. Hence, Ni_2Al_1-re460 with high hydrogenation and deoxygenation activities achieve complete HDO of EHL. With the enhancement of the reduction condition, the size of metal Ni in the catalyst increases, and the amount of Lewis acid sites and specific surface area decreases. Hence, NiAl-LDH reduced at a low temperature, i.e., Ni_2Al_1-re460, has a higher HDO activity than Ni_2Al_1-re520 and Ni_2Al_1-re580.

With the increase of the number of runs, NiO is gradually reduced to Ni, resulting in the growth of Ni particles. When the average size of Ni particles reaches 12.56 nm in 4^{th} run, the hydrogenation activity of the catalyst is significantly reduced and lignin fragments are strongly adsorbed on the large Ni particles. These adsorbed lignin fragments cannot be hydrogenated and further converted to condensed structures and char [48], which will also cover the active sites of catalysts, aggravating catalyst deactivation.

5. Conclusions

The Ni catalyst derived from NiAl-LDH was employed for the direct HDO reaction of EHL. NiAl-LDH is synthesized when the molar ratio of Ni and Al is 2. The NiAl-LDH reduced at 460 °C (Ni_2Al_1-re460) shows the highest activity among the catalysts tested, due to the high number of acidic Lewis sites, small size metal Ni particles and a large specific surface area. At optimized reaction conditions (320 °C, 3 MPa H_2, 6 h), EHL is completely converted and hydro-deoxygenated. The calorific value of liquid products is up to 42.5 MJ kg^{-1}, much higher than that of liquid products obtained without a catalyst.

The reaction pathways are proposed. EHL is firstly depolymerized via thermal decomposition process. CYH solvent dissolves lignin fragments and monomers. The catalyst further depolymerizes fragments and oligomers and converts phenolic monomers and dimers to cycloalkanes. The HDO of lignin fragments to cycloalkanes shifts the solubility equilibrium of lignin fragments in CYH, hindering their condensation to char.

The catalyst is reused up to three times without any loss of activity, and its deactivation is caused by the growth of Ni particles and active site coverage with highly absorbed species and char.

CRediT authorship contribution statement

Sang Yushuai: Writing – review & editing, Writing – original draft. **Jiao Hairui:** Writing – original draft. **Xu Guifeng:** Formal analysis, Data curation. **Chen Hong:** Funding acquisition. **Li Yongdan:** Supervision.

Declaration of Competing Interest

The authors declare that they have no known competing financial interests or personal relationships that could have appeared to influence the work reported in this paper.

Data Availability

The data that has been used is confidential.

Acknowledgments

This project has received funding from the European Union's Horizon 2020 research and innovation programme under grant agreement No 101006744. The content presented in this document represents the views of the authors, and the European Commission has no liability in respect of the content. This work was also supported by the National Natural Science Foundation of China (21808163).

Appendix A. Supporting information

Supplementary data associated with this article can be found in the online version at doi:10.1016/j.cattod.2024.114542.

References

[1] C. Li, X. Zhao, A. Wang, G.W. Huber, T. Zhang, Catalytic transformation of lignin for the production of chemicals and fuels, Chem. Rev. 115 (2015) 11559–11624.
[2] Z. Sun, B. Fridrich, A. de Santi, S. Elangovan, K. Barta, Bright side of lignin depolymerization: toward new platform chemicals, Chem. Rev. 118 (2018) 614–678.
[3] N. Sarkar, S.K. Ghosh, S. Bannerjee, K. Aikat, Bioethanol production from agricultural wastes: an overview, Renew. Energ. 37 (2012) 19–27.
[4] S. Kim, B.E. Dale, Global potential bioethanol production from wasted crops and crop residues, Biomass-.-. Bioenergy 26 (2004) 361–375.
[5] D.S. Bajwa, G. Pourhashem, A.H. Ullah, S.G. Bajwa, A concise review of current lignin production, applications, products and their environmental impact, Ind. Crop. Prod. 139 (2019).
[6] R. Ma, W. Hao, X. Ma, Y. Tian, Y. Li, Catalytic ethanolysis of Kraft lignin into high-value small-molecular chemicals over a nanostructured alpha-molybdenum carbide catalyst, Angew. Chem., Int. Ed. 53 (2014) 7310–7315.
[7] X. Ma, K. Cui, W. Hao, R. Ma, Y. Tian, Y. Li, Alumina supported molybdenum catalyst for lignin valorization: effect of reduction temperature, Bioresour. Technol. 192 (2015) 17–22.
[8] X. Ma, R. Ma, W. Hao, M. Chen, F. Iran, K. Cui, Y. Tian, Y. Li, Common pathways in ethanolysis of Kraft lignin to platform chemicals over molybdenum-based catalysts, ACS Catal. 5 (2015) 4803–4813.
[9] M. Chen, W. Hao, R. Ma, X. Ma, L. Yang, F. Yan, K. Cai, H. Chen, Y. Li, Catalytic ethanolysis of Kraft lignin to small-molecular liquid products over an alumina supported molybdenum nitride catalyst, Catal. Today 298 (2017) 9–15.
[10] M. Chen, X. Ma, R. Ma, Z. Wen, F. Yang, K. Cui, H. Chen, Y. Li, Ethanolysis of Kraft lignin over a reduction-modified MoO_3 catalyst, Ind. Eng. Chem. Res. 56 (2017) 14025–14033.
[11] F. Yan, R. Ma, X. Ma, K. Cui, K. Wu, M. Chen, Y. Li, Ethanolysis of Kraft lignin to platform chemicals on a MoC_{1-x}/Cu-$MgAlO_z$, catalyst, Appl. Catal. B-Environ. 202 (2017) 305–313.
[12] F. Mai, Z. Wen, Y. Bai, Z. Ma, K. Cui, K. Wu, F. Yan, H. Chen, Y. Li, Selective conversion of enzymatic hydrolysis lignin into alkylphenols in supercritical ethanol over a WO_3/γ-Al_2O_3 catalyst, Ind. Eng. Chem. Res. 58 (2019) 10255–10263.
[13] Y. Sang, M. Chen, F. Yan, K. Wu, Y. Bai, Q. Liu, H. Chen, Y. Li, Catalytic depolymerization of enzymatic hydrolysis lignin into monomers over an unsupported nickel catalyst in supercritical ethanol, Ind. Eng. Chem. Res. 59 (2020) 7466–7474.
[14] Y. Sang, K. Wu, Q. Liu, Y. Bai, H. Chen, Y. Li, Catalytic ethanolysis of enzymatic hydrolysis lignin over an unsupported nickel catalyst: The effect of reaction conditions, Energy Fuels 35 (2021) 519–528.
[15] Y. Ma, Y. Sang, K. Wu, Q. Liu, H. Chen, Y. Li, Selective production of 2-(tert-butyl)-3-methylphenol from depolymerization of enzymatic hydrolysis lignin with MoS_2 catalyst, Catal. Today 408 (2023) 194–203.
[16] H. Ma, W. Zhang, D. Chen, Catalytic hydrodeoxygenation of phenolic compounds over Ru-MoFeP/Al_2O_3 catalyst, Catal. Today 408 (2023) 50–57.
[17] Y. Liu, G. Cheng, E. Baráth, H. Shi, J.A. Lercher, Alkylation of lignin-derived aromatic oxygenates with cyclic alcohols on acidic zeolites, Appl. Catal. B-Environ. 281 (2021).
[18] S. Kim, E.E. Kwon, Y.T. Kim, S. Jung, H.J. Kim, G.W. Huber, J. Lee, Recent advances in hydrodeoxygenation of biomass-derived oxygenates over heterogeneous catalysts, Green. Chem. 21 (2019) 3715–3743.
[19] J.H. Zhang, J.M. Sun, Y. Wang, Recent advances in the selective catalytic hydrodeoxygenation of lignin-derived oxygenates to arenes, Green. Chem. 22 (2020) 1072–1098.
[20] H. Wei, Z. Wang, H.J.G.C. Li, Sustainable biomass hydrodeoxygenation in biphasic systems, Green. Chem. 24 (2022) 1930–1950.
[21] J. Kong, M. He, J.A. Lercher, C. Zhao, Direct production of naphthenes and paraffins from lignin, Chem. Commun. 51 (2015) 17580–17583.
[22] S. Kasakov, H. Shi, D.M. Camaioni, C. Zhao, E. Barath, A. Jentys, J.A. Lercher, Reductive deconstruction of organosolv lignin catalyzed by zeolite supported nickel nanoparticles, Green. Chem. 17 (2015) 5079–5090.
[23] J. Kong, B. Li, C. Zhao, Tuning Ni nanoparticles and the acid sites of silica-alumina for liquefaction and hydrodeoxygenation of lignin to cyclic alkanes, RSC Adv. 6 (2016) 71940–71951.
[24] Z. Luo, J. Kong, B. Ma, Z. Wang, J. Huang, C. Zhao, Liquefaction and hydrodeoxygenation of polymeric lignin using a hierarchical Ni microreactor catalyst, ACS Sustain. Chem. Eng. 8 (2020) 2158–2166.
[25] Z. Luo, S. Qin, S. Chen, Y. Hui, C. Zhao, Selective conversion of lignin to ethylbenzene, Green. Chem. 22 (2020) 1842–1850.

[26] S. Qin, B. Li, Z. Luo, C. Zhao, The conversion of a high concentration of lignin to cyclic alkanes by introducing Pt/HAP into a Ni/ASA catalyst, Green. Chem. 22 (2020) 2901–2908.
[27] Q. Xia, Z. Chen, Y. Shao, X. Gong, H. Wang, X. Liu, S.F. Parker, X. Han, S. Yang, Y. Wang, Direct hydrodeoxygenation of raw woody biomass into liquid alkanes, Nat. Commun. 7 (1) (2016) 10.
[28] L. Dong, L. Lin, X. Han, X. Si, X. Liu, Y. Guo, F. Lu, S. Rudić, S.F. Parker, S. Yang, Y. Wang, Breaking the limit of lignin monomer production via cleavage of interunit Carbon–Carbon linkages, Chem 5 (2019) 1521–1536.
[29] Y. Guo, Y. Jing, Q. Xia, Y. Wang, NbO_x-based catalysts for the activation of C–O and C–C bonds in the valorization of waste carbon resources, Acc. Chem. Res. 55 (2022) 1301–1312.
[30] H. Wang, H. Wang, E. Kuhn, M.P. Tucker, B. Yang, Production of jet fuel-range hydrocarbons from hydrodeoxygenation of lignin over super Lewis acid combined with metal catalysts, ChemSusChem 11 (2018) 285–291.
[31] Q. Liu, Y. Bai, H. Chen, M. Chen, Y. Sang, K. Wu, Z. Ma, Y. Ma, Y. Li, Catalytic conversion of enzymatic hydrolysis lignin into cycloalkanes over a gamma-alumina supported nickel molybdenum alloy catalyst, Bioresour. Technol. 323 (2021) 124634.
[32] K. Barta, T.D. Matson, M.L. Fettig, S.L. Scott, A.V. Iretskii, P.C. Ford, Catalytic disassembly of an organosolv lignin via hydrogen transfer from supercritical methanol, Green. Chem. 12 (2010) 1640–1647.
[33] X. Huang, T.I. Koranyi, M.D. Boot, E.J. Hensen, Catalytic depolymerization of lignin in supercritical ethanol, ChemSusChem 7 (2014) 2276–2288.
[34] Y. Bai, K. Cui, Y. Sang, K. Wu, F. Yan, F. Mai, Z. Ma, Z. Wen, H. Chen, M. Chen, Y. Li, Catalytic Depolymerization of a lignin-rich corncob residue into aromatics in supercritical ethanol over an alumina-supported NiMo alloy catalyst, Energy Fuels 33 (2019) 8657–8665.
[35] J. He, C. Zhao, J.A. Lercher, Ni-catalyzed cleavage of aryl ethers in the aqueous phase, J. Am. Chem. Soc. 134 (2012) 20768–20775.
[36] F. Yan, Z. Wen, K. Wu, K. Cui, F. Mai, Z. Ma, Y. Sang, Y. Bai, H. Chen, Y. Li, Deoxyalkylation of guaiacol using haggite structured $V_4O_6(OH)_4$, Catal. Sci. Technol. 9 (2019) 1922–1932.
[37] K. Nakajima, R. Noma, M. Kitano, M. Hara, Titania as an early transition metal oxide with a high density of Lewis, Acid. sites Work. Water, J. Phys. Chem. C. 117 (2013) 16028–16033.
[38] Y. Wang, F. Wang, Q. Song, Q. Xin, S. Xu, J. Xu, Heterogeneous ceria catalyst with water-tolerant Lewis acidic sites for one-pot synthesis of 1,3-diols via Prins, Condens. Hydrolys. React., J. Am. Chem. Soc. 135 (2013) 1506–1515.
[39] K. Nakajima, R. Noma, M. Kitano, M. Hara, Selective glucose transformation by titania as a heterogeneous Lewis, Acid. Catal., J. Mol. Catal. A-Chem., 388- 389 (2014) 100–105.
[40] K.A. Jung, S.H. Woo, S.-R. Lim, J.M. Park, Pyrolytic production of phenolic compounds from the lignin residues of bioethanol processes, Chem. Eng. J. 259 (2015) 107–116.
[41] S. Zhou, Y. Xue, A. Sharma, X. Bai, Lignin valorization through thermochemical conversion: Comparison of hardwood, softwood and herbaceous lignin, ACS Sustain. Chem. Eng. 4 (2016) 6608–6617.
[42] Q. Song, F. Wang, J. Cai, Y. Wang, J. Zhang, W. Yu, J. Xu, Lignin depolymerization (LDP) in alcohol over nickel-based catalysts via a fragmentation–hydrogenolysis process, Energy Environ. Sci. 6 (2013) 94–1007.
[43] Y. Sang, H. Chen, M. Khalifeh, Y. Li, Catalysis and chemistry of lignin depolymerization in alcohol solvents-A review, Catal. Today 408 (2023) 168–181.
[44] L. Huang, F. Tang, P. Liu, W. Xiong, S. Jia, F. Hao, Y. Lv, H. Luo, Highly efficient and selective conversion of guaiacol to cyclohexanol over Ni-Fe/$MgAlO_x$: Understanding the synergistic effect between Ni-Fe alloy and basic sites, Fuel 327 (2022) 125115.
[45] V.O.O. Gonçalves, P.M. de Souza, T. Cabioc'h, V.T. da Silva, F.B. Noronha, F. Richard, Hydrodeoxygenation of m-cresol over nickel and nickel phosphide based catalysts, Influ. Nat. Act. phase Support, Appl. Catal. B-Environ. 219 (2017) 619–628.
[46] D.J. Rensel, S. Rouvimov, M.E. Gin, J.C. Hicks, Highly selective bimetallic FeMoP catalyst for C-O bond cleavage of aryl ethers, J. Catal. 305 (2013) 256–263.
[47] S.-K. Wu, P.-C. Lai, Y.-C. Lin, H.-P. Wan, H.-T. Lee, Y.-H. Chang, Atmospheric hydrodeoxygenation of guaiacol over alumina-, zirconia-, and silica-supported nickel phosphide catalysts, ACS Sustain. Chem. Eng. 1 (2013) 349–358.
[48] A. Shaw, X. Zhang, S. Jia, J. Fu, L. Lang, R.C. Brown, Mechanistic investigation of char growth from lignin monomers during biomass utilisation, Fuel Process. Technol. 239 (2023) 107556.